Mon. Not. R. Astron. Soc. **000**, 1–5 (2015) Printed 19 April 2015 (MN LATEX style file v2.2)

Scintillation Distance Measurements

Siqi Liu[1,3⋆], Ue-Li Pen[1,2]†, J-P Macquart[4]‡, Walter Brisken[5]§, Adam Deller[6]¶
[1] *Canadian Institute for Theoretical Astrophysics, University of Toronto, M5S 3H8 Ontario, Canada*
[2] *Canadian Institute for Advanced Research, Program in Cosmology and Gravitation*
[3] *Department of Astronomy and Astrophysics, University of Toronto, M5S 3H4, Ontario, Canada*
[4] *ICRAR-Curtin University of Technology, Department of Imaging and Applied Physics, GPO Box U1978, Perth, Western Australia 6102, USA*
[5] *National Radio Astronomy Observatory, P.O. Box O, Socorro, NM 87801, USA*
[6] *ASTRON, the Netherlands Institute for Radio Astronomy, Postbus 2, 7990 AA, Dwingeloo, The Netherlands*

19 April 2015

ABSTRACT
We show how interstellar scintillations, combined with VLBI measurements, can be used to measure distances. We apply the technique to archival data on PSR B0834+06, concluding that for this example the plasma lenses can be precisely modelled using the Pen and Levin (2014) inclined sheet model, resulting in two distinct lens planes. This data strongly favours the reconnection sheet model over turbulence as the primary source of pulsar scattering. A global conformal distance degeneracy exists which allows a rescaling of the absolute distance scale. This degeneracy is broken if the pulsar resides in a binary system, which is the case for most precision timing targets.

Key words: Pulsar

1 INTRODUCTION

Pulsars have long provided a rich source of astrophysical information due to their compact emission and predictable timing. One of the weakest measurements for most pulsars is their direct geometric distance. For some pulsars, timing parallax or VLBI parallax has resulted in direct distance determinations. For most pulsars, the distance is a major uncertainty for precision timing interpretations, including mass, moment of inertia, and gravitational wave direction (Boyle & Pen 2012).

Direct VLBI observation of PSR B0834+06 shows multiple images lensed by the interstellar plasma. Combining the angular positions and scintillation delays, the authors published the derived effective distance (Brisken et al. 2010) of approximately 1168 ± 23 pc for apexes whose time delays range from 0.1 ms to 0.4 ms, and 1121 ± 59 pc for 1 ms apexes. This represents a precise measurement compared to all other attempts to derive distances to this pulsar. This effective distance is a combination of pulsar-screen and earth-screen distances, and does not allow a separate determination of the individual distances. A binary pulsar system would in principle allow a breaking of this degeneracy (Pen & Levin 2014). One potential limitation is the precision to which the lensing model can be understood. In this paper, we demonstrate that the lensing screen consists of nearly parallel linear refractive structures, in two screens. The precise model confirms the one dimensional nature, and thus the small number of parameters that need to be measured to quantify the lensing screen.

⋆ E-mail: sqliu@cita.utoronto.ca
† E-mail: pen@cita.utoronto.ca
‡ E-mail:J.Macquart@curtin.edu.au
§ Email:wbrisken@aoc.nrao.edu
¶ E-mail:deller@astron.nl

2 LENSING

2.1 B0834+06

Our analysis is based on the reduced apex catalog from Brisken et al. (2010). Other information from each identified apex includes delay, delay rate, RA and dec, one for each of 4 8 MHz wide sub-bands, centering 314.5 MHz, 322.5 MHz, 328.5 MHz and 334.5 MHz. We mapped a total of 9 apexes from the 0.4 ms group, and 5 from the 1 ms group. This results in an estimation for the mean value and standard deviation, which are listed in Table 2.4. The time is calculated with $2\tau f/f_D$, which is equivalent to pulsar moving at 640pc plane from the original position to the lensed image position with the velocity calculated. How distance of the pulsar is related to the time delay and how velocity is related to the differential frequency is defined by the following equations:

$$\tau = \frac{D_{\rm e}\theta^2}{2c},$$
$$f_D = f \cdot \frac{\delta\tau}{dt},$$

where $D_{\rm e}$ is the effective distance, equivalent to the lens placing at the middle point of the pulsar: $D_{\rm e} = D_p D_s/(D_p - D_s)$.

A least square effective distance results in $D_e^M = 1017.1 \pm 2.8$ for the main 0.4 ms apexes and $D_e^S = 1243 \pm 64$ for the secondary 1 ms apexes. This seems to indicate that the secondary screen is closer to the pulsar. The error bars are large enough to allow them to be at the same distance, or perhaps a reverse distance ordering. In this paper, we present two analyses for comparison: equidistant, and at the best fit distances. In the first case, no direct distance measurement is possible, but it nevertheless illustrates a robust interpretation of the data.

2.2 Lens Solution

In order to interpret the data, we adopt the lensing model of Pen & Levin (2014). In the absence of a lens model, the fringe rate, delay and angular position cannot be uniquely related. In this model, the lensing is due to projected fold caustics of a thin sheet closely aligned to the line of sight.

Furthermore, if we know the distance of the pulsar is 640 pc by parallax, the screen where 0.4 ms scintellation points are refracted, D_s is equal to 392.8 pc. We know the position of the axis angle, with an α 25.2 degree west of north, and the positions of the 0.4 ms pile are calculated. They are marked out with the scatter points on the left sidde of Figure 2. Similarly, for 1 ms apexes, the D_s is equal to 422.5 pc. Thus, the degeneracy of the distance of the screen is broken.

For the positions of the 1 ms apexes. First, matching the θ-τ relation, which is plotted in Figure 1, we calculated the θ from observation τ. Second, we consider the point with the largest θ among this 1 ms group, which is called 5, share the same $\theta_\parallel$ with the point with the largest θ among the 0.4 ms group, which is called 6. Thus, the position of point 5, is determined. Third, to determine the position of the rest point $1-4$, we need to know the velocity of the pulsar, and then to fit the RA and dec to get the same differential frequency with the observation. To know the proper motion of the pulsar, we calculated the its component in two directions: $v_\parallel$ according to the differential frequency of point 6 in 0.4 ms; and $v_{\rm A5}$ (in the direction pointing from point 5 to A) according to the differential frequency of point 5. Fourth, we fit the position of the rest four points, with known proper motion of the pulsar. Then we fit a line to this five calculated points.

That is one lens model fitting. Knowing time delay τ , we can get the distance of the screen; knowing the position of point 5 and the differential frequency f_D, we can get the velocity of the pulsar; knowing the velocity and observation diffferential frequency, we can get the position of points $1-4$.

2.3 Discussion of one lens model

The 0.4 ms group lens solution appears consistent with the premise of the inclined sheet lensing model (Pen & Levin 2014).

For 1 ms group, the secondary lens only images a subset of the primary lens images. This could happen if the secondary lens screen is just under the critical inclination angle, such that only $3-\sigma$ waves lead to a fold caustic. If the primary lens were at a critical angle, the chance of encountering a somewhat less inclined system is of order unity. More surprising is the absence of a single refraction image of the pulsar, which is expected at position J. This could happen if the maximum refraction angle is just below critical, such that only rays on the appropriately aligned double refraction can form images. This scenario predicts that at frequencies just below 300 MHz, or a few weeks earlier in time, the pulsar should be seen at position J. We made a plot of the refraction angle β in the direction that is transverse to the first lens plane in Figure 5. From our calculation, it takes 22 days for the puslar to move from point 1 on the near screen to J, and it takes 44 days for the pulsar to move from point 5 on the near screen to J. The data spans about 10% in frequency, making it unlikely that single lens image J would not be seen due to the larger required refraction angle. Instead, we speculate that the fold caustic could have formed near double lens image 1, and thus only intersections with the closer lens plane caustic south of image 1 are double lensed.

2.4 Double lens model

The $v_\parallel$ to the plane should be equal. While for the calculated positions of 1 ms apexes, they do not. The plane where the light was refracted should be transverse to the line that connects the pulsar and the lensed image. For the approximately same time delay of the 5 points among 1 ms group, the lens where the image formed should be at the same distance away from us. The only reasonable plane is line that fits all these five points, marked with a solid line in Figure 2. However, in this senario, the screens cross each other, which is unrealistic for the structure of the interstellar medium.

Therefore, we consider another model candidate: the double lens model. Respective calculation shows that the light is first refracted by the far screen and then refracted by the near screen.

The first step is to calculate the position of J. We calculated the position of J by matching the time delay of point 2, point 4 and point 5. The result shows that the far lens is 425 pc away from us. And its position is marked in Figure 2. Because J is the pedal to the far screen, we made a line that is perpendicular to AJ, the solid line in Figure 2.

The second step is to find the matched pairs of those two lenses. By try and error, we found that the 5 points in 0.4 ms group that have the largest θ should be the candidates where the near lens lie. These five matched lines are marked with dot dash lines in Figure 2 and their values are listed in Table 2.4 the first two columns. They are the secondary screens, at a distance 392.8 pc away from us.

By using the refraction law, we solve the solutions in double lens model.And the solved positions are plotted in Figure 2, and respective time delays and differential fre-

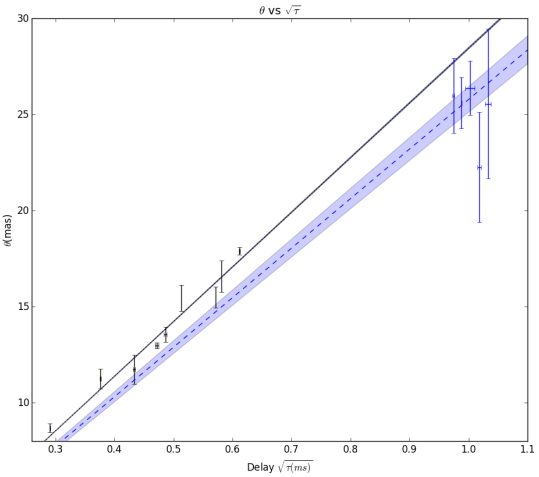

Figure 1. θ vs $\sqrt{\tau}$. The solid line is the fitted line of the 0.4ms positions, where $k = 28.51$ with an error region of $\sigma_k = 0.04$. The dashed lines are the fitted lines of the 1ms position, where $k = 25.78$ with an error region of $\sigma_k = 0.66$.

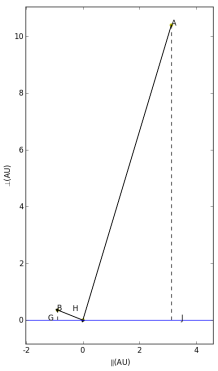

Figure 3. Refraction on the far lens. The x axis marks the distance in the direction that is parallel to the first lens, and the y axis marks the distance in the direction that is transverse to the first lens. A is the position of the pulsar. H is the first screen image. B is the secondary screen iamge. J is the pedal of A to the first screen, and G is the pedal of B to the first screen. According to refraction Law, $v_{\rm JH}$ and $v_{\rm HG}$ should be equal. In this case, $\theta_{\parallel}$ of the second lens equal -17.44 mas.

quencies are listed in Table 2.4. Figure 3 and Figure 4 are examples of how light are being refracted on the first lens plane and the second lens plane, with $\theta_{\parallel}$ equal to -17.44 mas of the secondary lens plane position.

3 POSSIBLE IMPROVEMENTS

We discuss several strategies which can improve on the solution accuracy. The single biggest improvement would be to monitor over a week, when the pulsar crosses each individual lens, including both lensing systems.

Angular resolution can be improved using longer baselines, for example adding a GMRT-GBT baseline doubles

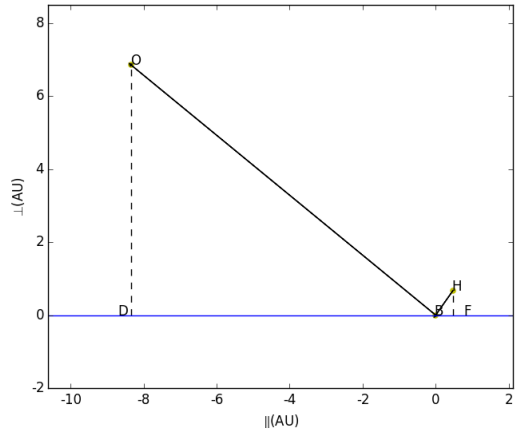

Figure 4. Refraction on the near lens. x axis marks the distance in the direction that is parallel to the second lens, and the y axis marks the distance in the direction that is transverse to the second lens. H is the first screen image. B is the second screen image. O is the position of the observer. F is the pedal of H to the second screen, and D is the pedal of O to the second screen. According to the refraction law, $v_{\rm FB}$ and $v_{\rm BD}$ should be equal. In this case, $\theta_{\parallel}$ of the second lens equal -17.44 mas.

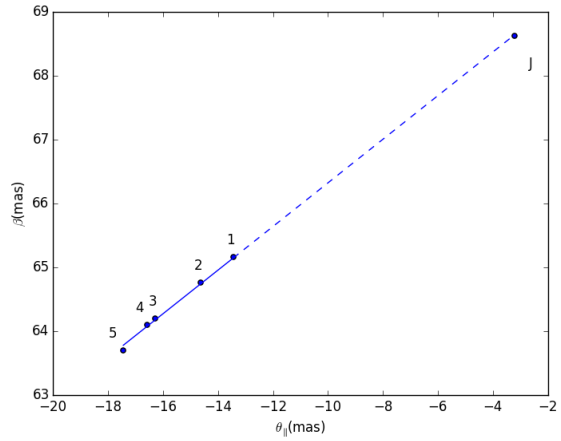

Figure 5. Injection velocity minus refracted velocity over the speed of light. J specifically marked in the paper.

the resolution. Observing at multiple frequencies over a longer period allows for a more precise measurement: when the pulsar is between two lenses, the refraction angle β is small, and one expects to see the lensing at higher frequency, where the resolution is higher, and distances between lenses positions can be measured to much higher accuracy.

Holographic techniques (Walker et al. 2008; Pen et al. 2014) may be able to measure delays, fringe rates, and VLBI positions sbstantially more accurately. Combining these techniques, the interstellar lensing could conceivably achieve distance measurements an order of magnitude better than the current published effective distance errors. This could bring most pulsar timing array targets into the coherent timing regime, enabling arc minute localization of gravitational wave sources, lifting any potential source confusion.

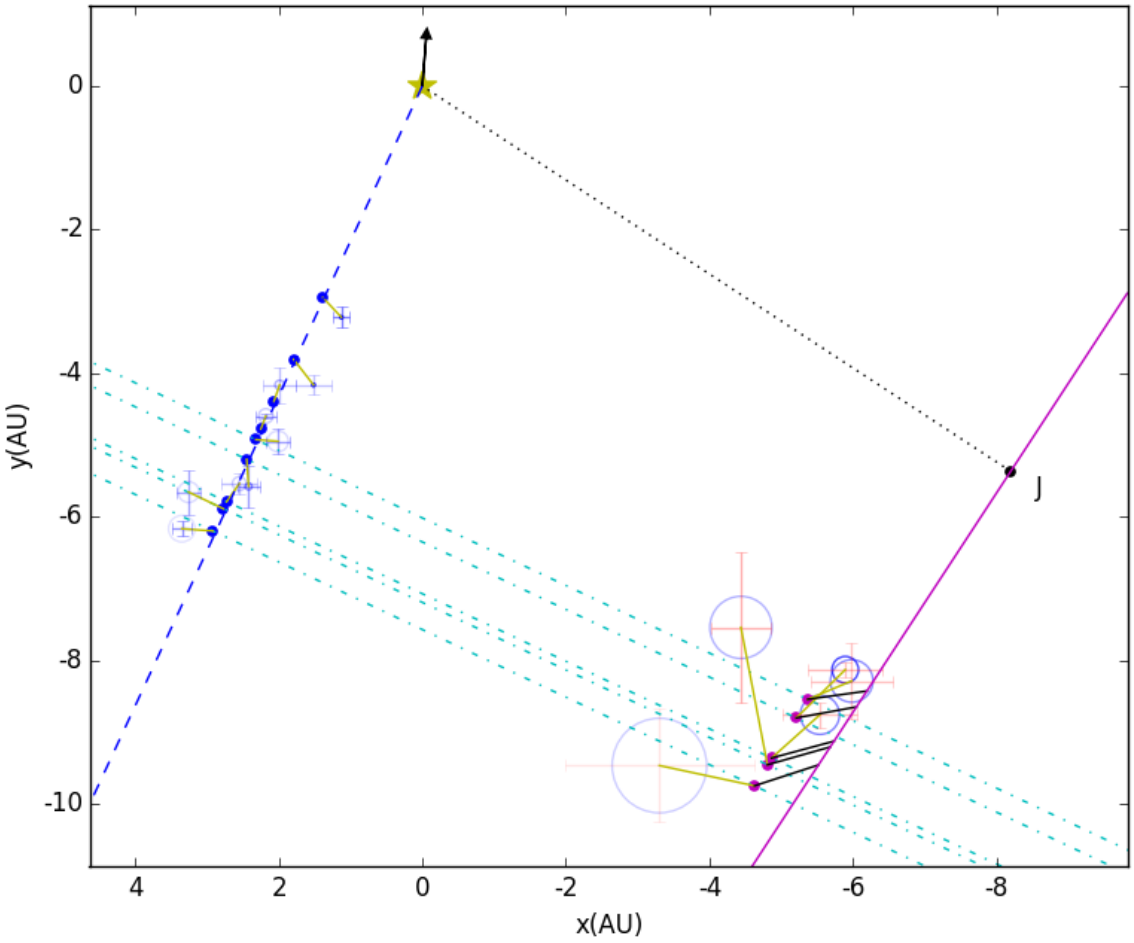

Figure 2. Observation data and calculated positions of 1 ms and 0.4 ms data of double lens model. In both apexes groups, the position of the screen locate at 392.8 pc and 425.0 pc. Blue points on the left side are the points that fitted from the f_D and τ of from the 0.4 ms apexes observation. Blue line is the fitted line of 0.4 ms apexes positions, with a angle α 25.2 degree west of north. The points lie on the left side with errorbars, are the observation points together with their sample errors; while the circles are plotted with population errors. Short solid lines between them are the matched positions of the observation positions and the calculated positions. The points on the right side are the points that fitted from the f_D and τ of the 1 ms apexes. Solid line is the fitted line of these positions. Those points with errorbars nearby are the observation points together with their sample errors, while the transparent circles are plotted with population errors. The dotted line on the top right side is vertical to the solid line. Short solid lines connect the observation points and the fitted positions. Middle lines connect the 0.4 ms and 1 ms fitted positions with the same $\theta_{\|}$. The proper motion of the pulsar is 192.6 km/s, with an angle γ 4.59 degree west of north, is marked with an arrow from a star at the top of the figure.

$\theta_\parallel$(mas)	f_D(mHz)	σ_{f_D}(mHz)	τ(ms)	σ_τ(ms)	RA(mas)	σ_{RA}(mas)	dec(mas)	σ_{dec}(mas)	time(day)
-8.29	-12.94	0.19	0.0845	0.0005	2.87	0.11	-8.201	0.088	49.9
-10.71	-16.80	0.28	0.14123	0.0009	3.86	0.07	-10.563	0.053	64.5
-12.36	-18.92	0.23	0.188	0.002	5.06	0.20	-10.58	0.13	74.4
-13.44	-20.40	0.49	0.222	0.003	5.55	0.30	-11.73	0.21	80.8
-13.86	-21.17	0.61	0.236	0.002	5.12	0.43	-12.56	0.31	83.4
-14.63	-22.32	0.47	0.2633	0.0003	6.16	0.14	-14.15	0.10	88.0
-16.29	-24.63	0.40	0.327	0.003	6.49	0.29	-14.06	0.20	98.0
-16.57	-24.94	0.44	0.338	0.0003	8.29	0.42	-14.37	0.32	99.7
-17.44	-26.09	0.36	0.3743	0.0006	8.53	0.52	-15.74	0.42	105
···	-35.06	0.52	0.950	0.002	-15.23	0.69	-21.06	0.70	202
···	-38.31	0.64	0.9763	0.0009	-15.02	0.48	-20.74	0.38	190
···	-40.17	0.55	1.0045	0.008	-14.14	0.66	-22.27	0.62	187
···	-41.27	0.54	1.037	0.003	-11.28	0.93	-19.2	1.1	188
···	-43.08	0.44	1.066	0.005	-8.4	1.7	-24.1	1.4	185

Table 1. 0.4ms and 1ms observation positions.

Lens 1 $\theta_\parallel(mas)$	Lens 2 $\theta_\parallel$(mas)	Observation τ(ms)	σ_τ(ms)	Calculated τ(ms)	Observation f_D(mHz)	σ_{f_D}(mHz)	Calculated f_D(mHz)
-13.86	-12.71	0.950	0.002	0.955	-35.06	0.52	-37.22
-14.63	-14.69	0.9763	0.0009	0.9763	-38.31	0.64	-38.31
-16.29	-15.78	1.005	0.008	1.0272	-40.17	0.55	-40.64
-16.57	-16.35	1.037	0.003	1.036	-41.27	0.54	-41.04
-17.44	-17.44	1.066	0.005	1.066	-43.08	0.44	-42.26

Table 2. comparison of the observation time delay and the differential frequency of the observation data and the calculated result of double lens model.

Ultimately, the precision of the lensing results would be limited by the fidelity of the lensing model. In the inclined sheet model, the images move along fold caustics. The straightness of these caustics depends on the inclination angle, which in turn depends on the amplitude of the surface waves.

4 CONCLUSIONS

We have applied the Pen and Levin Pen & Levin (2014) inclined sheet model to archival apex data of PSR B0834+06. The data is well fit by two linear lensing screens, with nearly plane-parallel geometry. This appears a natural consequence of very smooth reconnection sheets, and are an unlikely outcome of ISM turbulence. These results, if extrapolated to multi-epoch observations of binary systems, this might result in accurate distance determinations.

5 ACKNOWLEDGEMENTS

We thank NSERC for support.

REFERENCES

Boyle L., Pen U.-L., 2012, Phys. Rev. D, 86, 124028
Brisken W. F., Macquart J.-P., Gao J. J., Rickett B. J., Coles W. A., Deller A. T., Tingay S. J., West C. J., 2010, ApJ, 708, 232
Pen U.-L., Levin Y., 2014, MNRAS, 442, 3338
Pen U.-L., Macquart J.-P., Deller A. T., Brisken W., 2014, MNRAS, 440, L36
Walker M. A., Koopmans L. V. E., Stinebring D. R., van Straten W., 2008, MNRAS, 388, 1214